

**Strain-temperature phase diagram of BaZrO<sub>3</sub> with antiferrodistortive distortions**Jingtong Zhang <sup>1</sup>, Yajun Zhang,<sup>2</sup> Tao Xu,<sup>3</sup> and Jie Wang <sup>1,4,\*</sup><sup>1</sup>*Department of Engineering Mechanics, School of Aeronautics and Astronautics, Zhejiang University, 38 Zheda Road, Hangzhou 310027, China*<sup>2</sup>*Department of Mechanics and Engineering Sciences, College of Civil Engineering and Mechanics, Lanzhou University, Lanzhou, Gansu 730000, People's Republic of China*<sup>3</sup>*Ningbo Institute of Materials Technology and Engineering, Chinese Academy of Sciences, Ningbo 315201, China*<sup>4</sup>*Key Laboratory of Soft Machines and Smart Devices of Zhejiang Province, Zhejiang University, 38 Zheda Road, Hangzhou 310027, China*

(Received 2 September 2020; revised 6 December 2020; accepted 15 December 2020; published 22 January 2021)

Barium zirconate (BaZrO<sub>3</sub>) has attracted increasing attention due to its distinguished dielectric property and high chemical stability. As one kind of perovskite oxide, BaZrO<sub>3</sub> often exhibits a delicate interplay of lattice distortions and strain. In this work, the effect of strain on the ferroelectric and antiferrodistortive distortions in BaZrO<sub>3</sub> thin films is investigated at finite temperature by using density functional theory calculations and the first-principles based effective Hamiltonian method. It is found that due to the delicate balance between antiferrodistortive and ferroelectric distortions, polarization in BaZrO<sub>3</sub> thin films at absolute zero kelvin can be activated only under an in-plane tensile strain larger than 3.0%. The rotation of oxygen octahedra (antiferrodistortive distortion) is along the out-of-plane direction under the compressive strain and small tensile strain, whereas it changes to the in-plane direction when the tensile strain is larger than 0.3%. When the tensile strain increases to 4.1%, both rotation of oxygen octahedra and polarization are along the [110] direction. Furthermore, the temperature dependence of ferroelectric and antiferrodistortive distortions under different strains is investigated by using an effective Hamiltonian model. The strain-temperature phase diagram is calculated to identify the different distortions under different strains and temperatures.

DOI: [10.1103/PhysRevB.103.014113](https://doi.org/10.1103/PhysRevB.103.014113)**I. INTRODUCTION**

BaZrO<sub>3</sub> is one of the typical perovskites with high melting point, small thermal expansion coefficient, and distinguished dielectric property, which has a great potential in technological applications, such as a substrate for thin film deposition, microwave electronics, and high-temperature proton conductor [1–4]. However, unlike other ABO<sub>3</sub> perovskites such as BaTiO<sub>3</sub> and PbTiO<sub>3</sub>, ferroelectric distortion doesn't exist in BaZrO<sub>3</sub> when there is no external field [5], which causes BaZrO<sub>3</sub> to be more underappreciated than other perovskite materials. Nevertheless, the ferroelectric distortion appears when an in-plane strain is applied on BaZrO<sub>3</sub> [6,7], indicating that strain engineering may be used to tune the properties of BaZrO<sub>3</sub>.

Strain engineering has been an effective way of tuning properties of perovskite, such as phase transition temperature [8], piezoelectric properties [9], band gap [10], and so on. In general, the ferroelectric distortion in a perovskite is also sensitive to an external strain [11,12]. The coupling between ferroelectric polarization and strain provides a possible way to tune the ferroelectric properties in perovskite materials [13,14]. For example, the ferroelectric Curie temperature of BaTiO<sub>3</sub> can be enhanced to nearly 500 °C by strain, and the polarization is 250% higher than that of bulk BaTiO<sub>3</sub> [13].

Furthermore, an external strain can even induce ferroelectricity in paraelectric materials. For instance, the epitaxially strained SrTiO<sub>3</sub> exhibits ferroelectric polarization near room temperature [15]. The strain-temperature phase diagrams of SrTiO<sub>3</sub> have been constructed both experimentally and theoretically [16] to show the influence of strain and temperature. Meanwhile, a phase transition from cubic to tetragonal in BaZrO<sub>3</sub> has been observed under high hydrostatic pressure at room temperature [17,18], indicating that an external mechanical loading can control the phase transition in BaZrO<sub>3</sub>.

Several studies have been carried out to study the effect of external strain on the properties of BaZrO<sub>3</sub>. Previous first-principle calculations show that BaZrO<sub>3</sub> exhibits a paraelectric to ferroelectric transition under both compressive and tensile strain, and the dielectric constant is significantly enhanced [7]. Under the strain of −4%, the predicted polarization has the value of 34 μC/cm<sup>2</sup>, which is larger than the spontaneous polarization of BaTiO<sub>3</sub>. In the previous first-principles calculations [7], however, only ferroelectric distortion has been considered and other lattice distortions are excluded, which is often coupled with polarization. Furthermore, previous calculations are conducted only at zero temperature.

To predict the properties of perovskites at finite temperature, the first-principles-based effective Hamiltonian method is an effective way [19,20], which has been employed to study the phase diagram of many ferroelectric materials such as Ba<sub>x</sub>Sr<sub>1-x</sub>TiO<sub>3</sub> [21], BaTiO<sub>3</sub> [22], PbZr<sub>x</sub>Ti<sub>1-x</sub>O<sub>3</sub> [23–25],

\*jw@zju.edu.cn

NaNbO<sub>3</sub> [26], PbZrO<sub>3</sub> [27], BiFeO<sub>3</sub> [28,29], and so on. Since the ferroelectricity in perovskites arises from the ferroelectric lattice distortion, i.e., the relative displacement of atoms, it can be treated as a degree of freedom in the effective Hamiltonian method. In addition to the ferroelectric lattice distortion, there are also other kinds of lattice distortions that do not produce polarization in the perovskite, such as rotation and tilting of oxygen octahedra (antiferrodistortive distortion), Jahn-Teller distortion [30], and breathing distortion [31,32]. Among them, the rotation of oxygen octahedra has been reported to exist in many perovskite materials. By taking consideration of oxygen octahedral rotation, Bellaiche *et al.* confirmed the existence of a monoclinic *Cc* phase and a rhombohedral *R3c* phase in Pb(Zr, Ti)O<sub>3</sub> [25], which doesn't appear when the oxygen octahedral rotation is absent [24]. Although the rotation of oxygen octahedra has also been reported to exist in BaZrO<sub>3</sub> [5], none of the previous theoretical calculations have considered the role of the rotation of oxygen octahedra in the strain-temperature phase diagram, to the best of our knowledge. Up to now, how the rotation of oxygen octahedra interacts with polarization induced by strain and how temperature will influence these lattice distortions are still unknown for BaZrO<sub>3</sub>. Thus, it is necessary to introduce the rotation of oxygen octahedra as a degree of freedom into the effective Hamiltonian method and investigate its influence on the ferroelectric properties of BaZrO<sub>3</sub> at finite temperatures.

In this work, the effect of strain on the ferroelectric and antiferrodistortive (AFD) distortions in BaZrO<sub>3</sub> is investigated at finite temperature using density functional theory (DFT) calculations and first-principles based effective Hamiltonian method. First, the ferroelectric and AFD of BaZrO<sub>3</sub> under in-plane epitaxial strain are studied. Results from the DFT calculation show that only a relatively sizeable tensile strain can induce ferroelectric polarization. Second, the temperature dependence of AFD and ferroelectric polarization under different strains are investigated by the effective Hamiltonian method. Finally, a full strain-temperature phase diagram is constructed to identify the AFD and ferroelectric polarization in BaZrO<sub>3</sub> under different temperatures and strains.

## II. METHODOLOGY

### A. DFT calculations

First-principles calculations are performed to obtain potential energy surface and phonon dispersion of BaZrO<sub>3</sub> at absolute zero. The Vienna *ab initio* simulation package (VASP) is employed with LDA as exchange-correlation potential in the calculations. The following valence electrons for Ba(5s<sup>2</sup>5p<sup>6</sup>6s<sup>2</sup>), Zr(4s<sup>2</sup>4p<sup>6</sup>4d<sup>2</sup>5s<sup>2</sup>), and O(2s<sup>2</sup>2p<sup>4</sup>) ions are used, with an 850-eV plane-wave cutoff. The Brillouin zone is sampled using an 8×8×8 Monkhorst-Pack *k*-point mesh. The cubic BaZrO<sub>3</sub> is first fully relaxed until the Hellmann-Feynman forces on each atom is converged to be less than 10<sup>-3</sup> eV/Å. The calculated lattice parameter for cubic BaZrO<sub>3</sub> is 7.863 34 bohrs, which agrees well with other first-principles studies [6] and the experimental value obtained at 10 K (7.9198 bohrs) [5]. Based on the obtained lattice parameters, phonon dispersion curves are computed using the PHONOPY program code [33], in which the linear response

method based on the density functional perturbation theory (DFPT) is employed [34]. The rotation of oxygen octahedra which is associated with the unstable mode in phonon spectrum is considered as the degree of freedom while building an effective Hamiltonian model for BaZrO<sub>3</sub>.

The potential energy surfaces as a function of polarization are calculated for BaZrO<sub>3</sub> with and without the rotation of oxygen octahedra under different in-plane strains. The structure is fully relaxed until the Hellmann-Feynman force on each atom is converged to be lower than 10<sup>-3</sup> eV/Å. The displacement of atoms relative to the cubic structure is increased or decreased by changing the amplitude of different modes to achieve the energies under different polarizations. Similarly, the rotation of oxygen octahedra is added to each structure and the potential energy surface with oxygen octahedral rotation is obtained.

### B. First-principles-based effective Hamiltonian method

Based on DFT results, an effective Hamiltonian model is constructed to study BaZrO<sub>3</sub>. The effective Hamiltonian model has four degrees of freedom: (1) the Ba centered dimensionless variable  $\mathbf{v}$ , which is used to describe inhomogeneous strain  $\boldsymbol{\eta}_I$ ; (2) the Zr centered polar mode  $\mathbf{u}$ , which is associated with ferroelectric distortion; (3) the homogeneous strain tensor  $\boldsymbol{\eta}_H$ ; (4) the Zr centered AFD mode  $\boldsymbol{\omega}$  that represents the rotation of oxygen octahedra. The  $\boldsymbol{\omega}$  used here is a dimensionless quantity. It represents the ratio of the displacement of oxygen atoms to that under zero strain at 0 K. The total energy of BaZrO<sub>3</sub> includes two parts:

$$E^{\text{tot}} = E^{\text{FE}}(\{\mathbf{u}\}, \{\boldsymbol{\eta}\}) + E^{\text{AFD}}(\{\boldsymbol{\omega}\}, \{\mathbf{u}\}, \{\boldsymbol{\eta}\}), \quad (1)$$

where  $E^{\text{FE}}$  is the energy associated with polar modes, elastic deformations, and their couplings, while  $E^{\text{AFD}}$  is the energy associated with AFD modes and their interactions with polar mode and strain.  $\boldsymbol{\eta} = \boldsymbol{\eta}_I + \boldsymbol{\eta}_H$  represents the strain, which includes both homogeneous and inhomogeneous strain.  $E^{\text{FE}}$  can be expanded as [19]

$$E^{\text{FE}} = E^{\text{self}}(\{\mathbf{u}\}) + E^{\text{dpl}}(\{\mathbf{u}\}) + E^{\text{short}}(\{\mathbf{u}\}) + E^{\text{elas}}(\{\boldsymbol{\eta}\}) + E^{\text{int}}(\{\mathbf{u}\}, \{\boldsymbol{\eta}\}). \quad (2)$$

The first term in Eq. (2),  $E^{\text{self}}$ , is the polar mode self-energy, which represents the energy of polar mode without interaction with other polar modes. It can be expressed by

$$E^{\text{self}}(\{\mathbf{u}\}) = \sum_i [\kappa_2 u_i^2 + \alpha_2 u_i^4 + \gamma (u_{i,x}^2 u_{i,y}^2 + u_{i,y}^2 u_{i,z}^2 + u_{i,x}^2 u_{i,z}^2)], \quad (3)$$

where  $u_i = |\mathbf{u}_i|$ ; it means the amplitude of polar mode on the *i* th site.  $u_{i,x}$  means the component of the polar mode in the *x* direction on the *i* th site. The coefficients of  $\kappa_2$ ,  $\alpha_2$ , and  $\gamma$  need to be determined from first-principles calculations.

The second term  $E^{\text{dpl}}$  is the long-range dipole-dipole interaction. It can be expressed as

$$E^{\text{dpl}}(\{\mathbf{u}\}) = \frac{Z^{*2}}{\varepsilon_\infty} \sum_{i < j} \frac{\mathbf{u}_i \cdot \mathbf{u}_j - 3(\hat{\mathbf{R}}_{ij} \cdot \mathbf{u}_i)(\hat{\mathbf{R}}_{ij} \cdot \mathbf{u}_j)}{R_{ij}^3}, \quad (4)$$

where  $\mathbf{R}_{ij} = \mathbf{R}_i - \mathbf{R}_j$ ;  $Z^*$  and  $\varepsilon_\infty$  are the Born effective charge and optical dielectric constant, respectively.

The third term,  $E^{\text{short}}$ , is the short interaction. Since this energy decays rapidly with distance, we only consider the interactions between two neighbor polar modes that share the same Ba atom. The dipole-dipole interaction is excluded from this part. It can be written as

$$E^{\text{short}}(\{\mathbf{u}\}) = \frac{1}{2} \sum_{i \neq j} \sum_{\alpha\beta} J_{ij,\alpha\beta} u_{i,\alpha} u_{j,\beta}. \quad (5)$$

Here,  $u_{i,\alpha}$  is the  $\alpha$  component of polar mode on the  $i$  th site, while  $u_{j,\beta}$  is the  $\beta$  component on the  $j$  th site, and  $\alpha$  and  $\beta$  denote the Cartesian components.  $J_{ij,\alpha\beta}$  is the parameter for the short interaction between them.

The fourth term,  $E^{\text{elas}}$ , is the elastic energy, which includes both inhomogeneous and homogeneous strain:

$$E^{\text{elas}}(\{\boldsymbol{\eta}\}) = \sum_i \left\{ \frac{1}{2} B_{11} (\eta_{i,1}^2 + \eta_{i,2}^2 + \eta_{i,3}^2) + B_{12} (\eta_{i,1} \eta_{i,2} + \eta_{i,2} \eta_{i,3} + \eta_{i,1} \eta_{i,3}) + \frac{1}{2} B_{44} (\eta_{i,4}^2 + \eta_{i,5}^2 + \eta_{i,6}^2) \right\}, \quad (6)$$

$$E^{\text{AFD}}(\{\boldsymbol{\omega}\}, \{\mathbf{u}\}, \{\boldsymbol{\eta}\}) = E^{\omega\text{-self}}(\{\boldsymbol{\omega}\}) + E^{\omega\text{-short}}(\{\boldsymbol{\omega}\}) + E^{\omega\text{-u-int}}(\{\boldsymbol{\omega}\}, \{\mathbf{u}\}) + E^{\omega\text{-}\eta\text{-int}}(\{\boldsymbol{\omega}\}, \{\boldsymbol{\eta}\}). \quad (8)$$

The first term,  $E^{\omega\text{-self}}$ , can be read as

$$E^{\omega\text{-self}} = \sum_i \left[ \kappa_A \omega_i^2 + \alpha_A \omega_i^4 + \beta_A \omega_i^6 + \gamma_A (\omega_{i,x}^2 \omega_{i,y}^2 + \omega_{i,x}^2 \omega_{i,z}^2 + \omega_{i,y}^2 \omega_{i,z}^2) + \gamma'_A (\omega_{i,x}^2 \omega_{i,y}^4 + \omega_{i,x}^2 \omega_{i,z}^4 + \omega_{i,y}^2 \omega_{i,z}^4 + \omega_{i,y}^4 \omega_{i,x}^2 + \omega_{i,z}^2 \omega_{i,y}^4 + \omega_{i,z}^4 \omega_{i,x}^2) \right], \quad (9)$$

where  $\omega_i = |\boldsymbol{\omega}_i|$ , and  $\omega_{i,x}$  is the  $x$  component of  $\omega_i$ , which represents the rotation along the  $x$  axis. This term is truncated at sixth order instead of fourth order to guarantee convergence in Monte Carlo simulation.

The second term,  $E^{\omega\text{-short}}$ , is the short interactions between two neighbor AFD modes that share the same oxygen atom. It can be written as

$$E^{\omega\text{-short}} = \sum_{ij} \sum_{\alpha\beta} K_{ij\alpha\beta} \omega_{i,\alpha} \omega_{j,\beta} + K'_{ij\alpha\beta} \omega_{i,\alpha}^2 \omega_{j,\beta}^2, \quad (10)$$

where  $K_{ij\alpha\beta} = \delta_{\alpha\beta} (|R_{ij,\alpha}|(k_{12} - k_{11}) + k_{11}) + (1 - \delta_{\alpha\beta}) (|R_{ij,\alpha}|(k_{13} - k_{14}) + k_{14})$ , and  $K'_{ij\alpha\beta} = k_{21}$ .  $K_{ij\alpha\beta}$  and  $K'_{ij\alpha\beta}$  are the parameters between the  $\alpha$  component of AFD mode at site  $i$ th, with  $\beta$  component of AFD mode at site  $j$ th.

The third term,  $E^{\omega\text{-u-int}}$ , is the interactions between AFD modes and polar modes. It only considers the biquadratic term and can be expressed as

$$E^{\omega\text{-u-int}}(\{\boldsymbol{\omega}\}, \{\mathbf{u}\}) = \sum_{i,j} \sum_{\alpha\beta\gamma\delta} E_{\alpha\beta\gamma\delta} \omega_{i,\alpha} \omega_{j,\beta} u_{j,\gamma} u_{i,\delta}. \quad (11)$$

The last term,  $E^{\omega\text{-}\eta\text{-int}}$ , is the coupling between strain and AFD modes. It also includes both inhomogeneous strain and homogeneous strain. It can be read as

$$E^{\omega\text{-}\eta\text{-int}}(\{\boldsymbol{\omega}\}, \{\boldsymbol{\eta}\}) = \sum_i \sum_{k\alpha\beta} C_{k\alpha\beta} \eta_{i,k} \omega_{i,\alpha} \omega_{j,\beta}. \quad (12)$$

where  $\eta_{i,k}$  ( $k = 1, 2, \dots, 6$ ) is the  $k$ -th component of total strain  $\boldsymbol{\eta}$  at the site  $i$ th.  $B_{11}$ ,  $B_{12}$ , and  $B_{44}$  are the elastic constants.

The fifth term,  $E^{\text{int}}$ , is the interaction energy between polar mode and strain. It can be read as

$$E^{\text{int}}(\{\mathbf{u}\}, \{\boldsymbol{\eta}\}) = \frac{1}{2} \sum_i \sum_{k\alpha\beta} B_{k\alpha\beta} \eta_{i,k} u_{i,\alpha} u_{i,\beta}, \quad (7)$$

in which  $B_{k\alpha\beta}$  is the coupling constant, and both homogeneous strain and inhomogeneous strain are included in  $\boldsymbol{\eta}$ . The formulation and physical meanings for the five energy terms of  $E^{\text{FE}}$  are the same as those in Ref. [19].

Although there are several energy terms for the AFD modes of the effective Hamiltonian model [26,27], only the terms with coefficients not close to zero are necessary for BaZrO<sub>3</sub>. Meanwhile, some high-order terms are introduced to ensure the convergence of the model, such as the sixth order in  $E^{\omega\text{-self}}$  and fourth order in  $E^{\omega\text{-short}}$ . The energy terms for AFD are given as follows:

All the parameters of BaZrO<sub>3</sub> used here are obtained from first-principles calculations and listed in Table I.

The Monte Carlo (MC) simulations are performed based on this effective Hamiltonian using a  $12 \times 12 \times 12$  supercell with period boundary condition. The in-plane strains from  $-5\%$  to  $5\%$  are considered to obtain the strain-temperature phase diagram of BaZrO<sub>3</sub> thin films. The equilibrate state under 0 K is achieved with  $10^6$  MC sweeps. After that, the model is heated up to 2000 K with a temperature step of 2 K. For each step,  $10^4$  MC sweeps are performed. At each MC step during the canonical MC simulation, we make a trial move on each  $\mathbf{u}$  in sequence, then each  $\mathbf{v}$ , then each  $\boldsymbol{\omega}$  in sequence, and then  $\boldsymbol{\eta}_H$ . The change of total energy after each trial movement is denoted by  $\Delta E_{\text{tot}}$ , and we can calculate the probability of this movement  $p$  by

$$p = \min \left[ 1, \exp \left( -\frac{\Delta E_{\text{tot}}}{k_B T} \right) \right], \quad (13)$$

where  $k_B$  is the Boltzmann constant and  $T$  is the temperature. The step size of degrees of freedom is adjusted during MC simulation to ensure the movement accepted by Eq. (13) is 0.2.

To verify the accuracy of the present model, the energy surfaces for the out-of-phase rotation from DFT calculation and the effective Hamiltonian model are given in Fig. 1. It is found that both energy surfaces agree well with each other,

TABLE I. Parameters of the effect Hamiltonian model for BaZrO<sub>3</sub> in atomic units using the notations of Ref. [20]. Energies are in hartree.

Parameters for FE		
Unit cell	$a_0$ 7.863 34 Bohr	
$E^{\text{dpl}}$	$Z^*$ 8.8158	$\epsilon_\infty$ 4.707
$E^{\text{self}}$	$\kappa_2$ 0.044 361 9 hartree/bohr <sup>2</sup>	$\gamma$ -0.010 56 hartree/bohr <sup>4</sup>
	$\alpha$ 0.030 99 hartree/bohr <sup>4</sup>	
$E^{\text{short}}$	$j_1$ -0.018 141 85 hartree/bohr <sup>2</sup>	$j_2$ 0.061 731 35 hartree/bohr <sup>2</sup>
	$j_3$ 0.006 018 8 hartree/bohr <sup>2</sup>	$j_4$ -0.004 257 5 hartree/bohr <sup>2</sup>
	$j_5$ 0.005 870 8 hartree/bohr <sup>2</sup>	$j_6$ 0.000 388 58 hartree/bohr <sup>2</sup>
	$j_7$ 0.000 388 58 hartree/bohr <sup>2</sup>	
$E^{\text{elas}}$	$B_{11}$ 5.7599 hartree	$B_{12}$ 1.454 35 hartree
	$B_{44}$ 1.483 hartree	
$E^{\text{int}}$	$B_{1xx}$ -1.403 714 hartree/bohr <sup>2</sup>	$B_{1yy}$ -0.061 93 hartree/bohr <sup>2</sup>
	$B_{4yz}$ -0.005 368 hartree/bohr <sup>2</sup>	
Parameters for AFD		
$E^{\omega\text{-self}}$	$\kappa_A$ 0.017 380 92 hartree	$\alpha_A$ -0.004 627 89 hartree
	$\beta_A$ 0.030 521 5 hartree	
	$\gamma_A$ 0.003 497 495 hartree	$\gamma'_A$ 0.123 04 hartree
$E^{\omega\text{-short}}$	$k_{11}$ 0.004 185 39 hartree	$k_{12}$ 0.001 545 02 hartree
	$k_{13}$ 0.001 198 75 hartree	
	$k_{14}$ 0.006 039 707 hartree	$k_{21}$ 0.004 356 5 hartree
$E^{\omega\text{-u-int}}$	$E_{xxxxA}$ 0.146 95 hartree/bohr <sup>2</sup>	$E_{xyyyA}$ 0.012 67 hartree/bohr <sup>2</sup>
	$E_{xyyyA}$ -0.108 77 hartree/bohr <sup>2</sup>	
$E^{\omega\text{-}\eta\text{-int}}$	$C_{1xxA}$ -0.7359 hartree	$C_{1yyA}$ 0.095 949 hartree
	$C_{4yzA}$ -0.008 108 hartree	

which indicates that the present model is precise to describe the energetic properties and phase transition of BaZrO<sub>3</sub>.

### III. RESULTS AND DISCUSSION

#### A. Rotation and polarization at the temperature of absolute zero

We first obtain the phonon spectrum of cubic BaZrO<sub>3</sub>. As is shown in Fig. 2(a), cubic BaZrO<sub>3</sub> doesn't exhibit instability at the  $\Gamma$  point, which is linked to the ferroelectric distortion

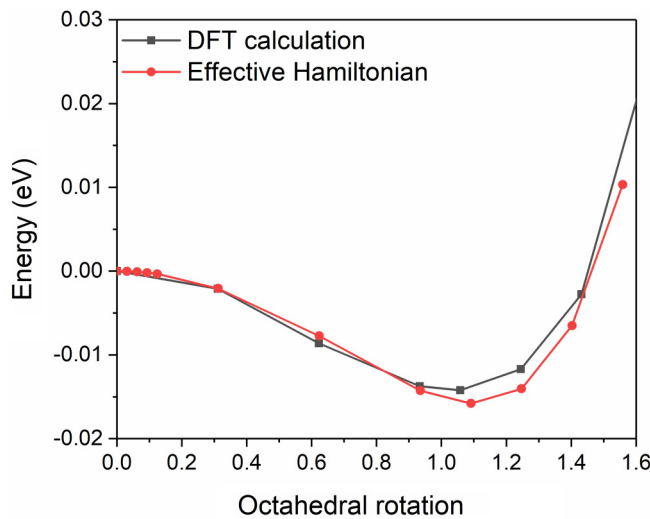


FIG. 1. The energy surfaces of out-of-phase rotation from the DFT calculation and the effective Hamiltonian. The two curves agree well with each other, which indicates the model is accurate to describe the energetic properties and phase transition of BaZrO<sub>3</sub>.

[35]. But there is an unstable phonon with  $R_{25}$  symmetry corresponding to the rotation of the oxygen octahedra [36]. The computed phonon spectrum is consistent with the results of previous calculations [37]. This unstable phonon  $R_{25}$  indicates that it is necessary to introduce the AFD mode (distortion) denoted by  $\omega$  into the effective Hamiltonian model. Furthermore, the phonon spectrum of BaZrO<sub>3</sub> under 4%, -2%, -4% in-plane strain are also calculated as shown in Figs. 2(b)–2(d). Instability at the  $\Gamma$  point appears under a relatively larger strain indicating the emergence of ferroelectricity in BaZrO<sub>3</sub> under both tensile and compressive strain and can be used to explain the ferroelectric distortion found in Ref. [7]. However, whether this ferroelectricity can coexist with oxygen octahedral rotation or not is still uncertain.

To investigate the interaction between ferroelectric and AFD distortions, we carried out several DFT calculations for the potential energy related to polarization with and without oxygen octahedra rotation. The strains are taken as 4% and -4%, respectively. The out-of-phase oxygen octahedral rotation is added on the [001] direction manually. The results are shown in Fig. 3. The polarizations are calculated from

$$P = \sum_{i=1}^5 \frac{\tilde{Z}_i^* \tilde{u}_i}{a^3}, \quad (14)$$

where  $i$  runs from 1 to 5; it represents five atoms for a perovskite unit cell.  $a$  is the lattice constant,  $\tilde{u}_i$  is the displacement of the  $i$ th atom in a unit cell, and  $\tilde{Z}_i^*$  is the Born effective charge for the  $i$ th atom. It should be noticed that the change of Born effective charge with epitaxial strain is not considered and the  $\tilde{Z}_i^*$  denotes the Born effective charge of the cubic phase. Although this simplification underesti-

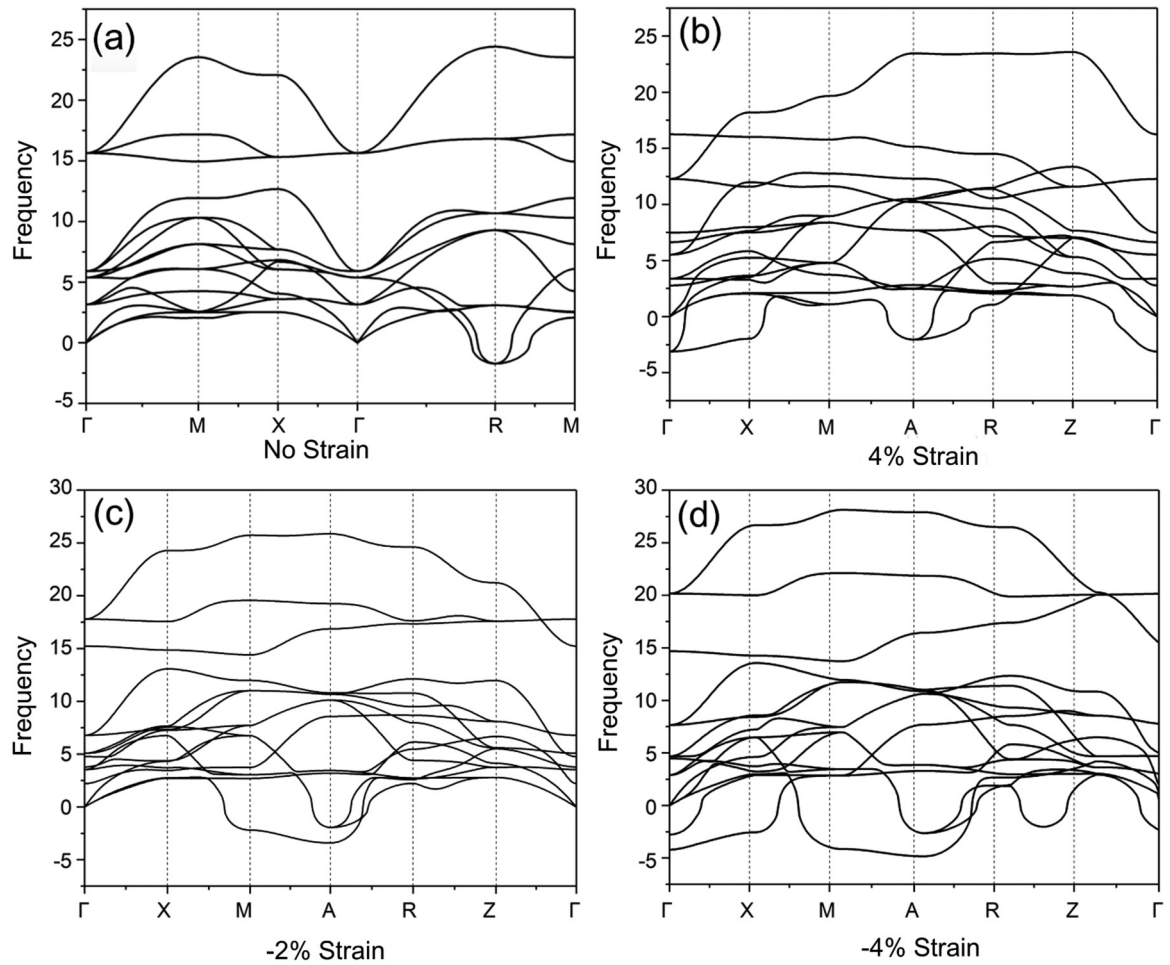


FIG. 2. Phonon spectrum of BaZrO<sub>3</sub> under different in-plane strains: (a) no strain; (b) the tensile strain of 4%; (c) the compressive strain of -2%; (d) the compressive strain of -4%. The symmetry point labels are  $\Gamma = (0, 0, 0)$ ,  $X = (0.5, 0, 0)$ ,  $M = (0.5, 0.5, 0)$ ,  $R = (0.5, 0.5, 0.5)$  in the cubic  $Pm\bar{3}m$  phase and  $\Gamma = (0, 0, 0)$ ,  $X = (0.5, 0, 0)$ ,  $M = (0.5, 0.5, 0)$ ,  $A = (0.5, 0.5, 0.5)$ ,  $Z = (0, 0, 0.5)$ ,  $R = (0, 0.5, 0.5)$  after in-plane strains are added. The R point in (a) and A points in (b)–(d) correspond to the out-of-phase rotation, while the  $\Gamma$  point corresponds to the ferroelectric distortion. The M points in (b)–(d) correspond to the in-phase rotation. The X point corresponds to the antiferroelectric distortion.

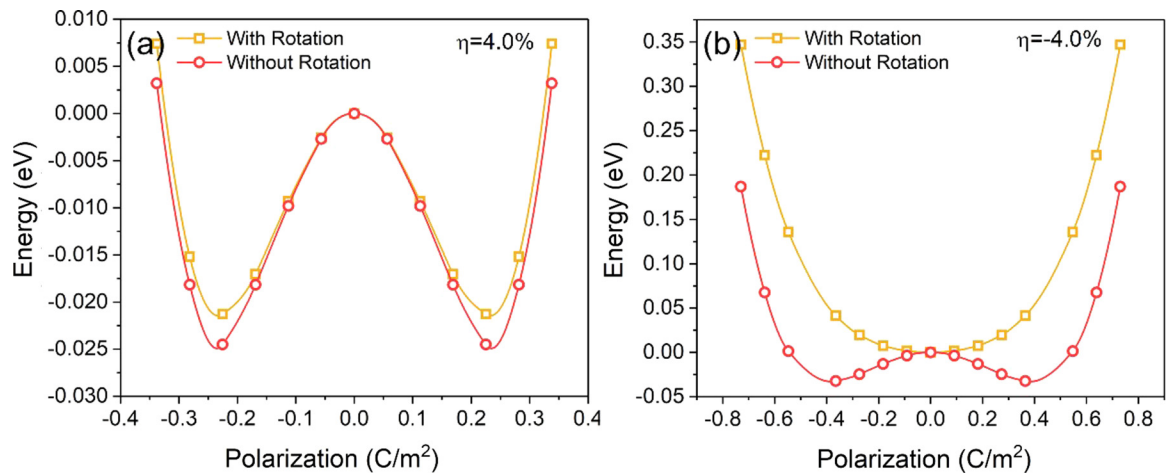


FIG. 3. The energy profiles for BaZrO<sub>3</sub> with and without the rotation of oxygen octahedron under (a) the tensile strain of 4%; and (b) the compressive of -4%. When the rotation of oxygen octahedron is considered, ferroelectric polarization is zero under a compressive strain.

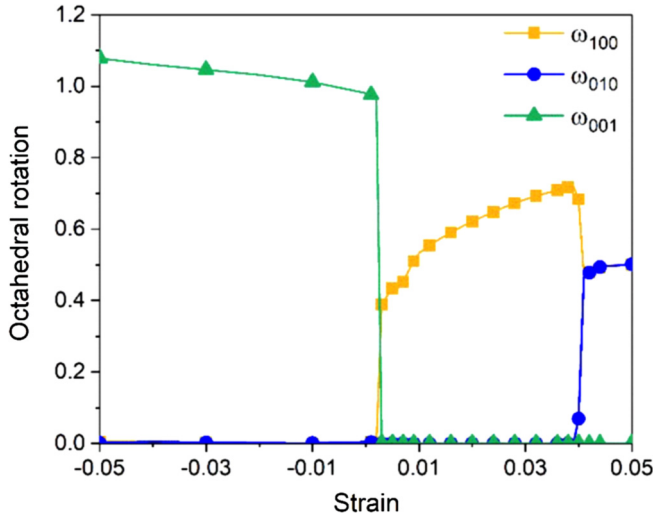


FIG. 4. Octahedral rotation changes with in-plane strain under 0 K from the effective Hamiltonian method.  $\omega_{100}$  represents the maximum in  $\omega_{100}$  and  $\omega_{010}$ . When the tensile strain is smaller than 0.3%, the rotation is in [001] direction, and it changes to [100] direction when the strain is in the range of 0.3–4.1%. When the strain is larger than 4.1%, the rotation on [010] direction has the same value as that on [100], which indicates that the rotation is along [110] direction.

mates dipole-dipole energy, its influence on the strain-induced polarization is very weak. The energy references in Fig. 3 are the cubic phase for  $\text{BaZrO}_3$  without rotation of oxygen octahedra and the  $I4/mcm$  phase for  $\text{BaZrO}_3$  with the rotation of oxygen octahedra. Without rotation of oxygen octahedra, the potential energy under both tensile and compressive strain shows a double well shape, which indicates polarization can be induced in  $\text{BaZrO}_3$ . However, after considering the rotation of oxygen octahedra, due to the interaction between polarization and rotation of oxygen octahedra, the double well under compressive strain turns into a single well. Meanwhile, the double well under tensile strain remains, as shown in Fig. 3. These results indicate that rotation of oxygen octahedra suppresses polarization. And the detailed relationship between oxygen octahedral rotation and strain-induced ferroelectricity are studied by the effective Hamiltonian method.

With the parameters listed in Table I, we perform effective Hamiltonian simulation for  $\text{BaZrO}_3$  with a  $12 \times 12 \times 12$  supercell, which is less than 5 nm. Due to the period boundary condition, the domains are not found in such a small supercell. The oxygen octahedral rotation and polarization with different in-plane strains are shown in Figs. 4 and 5. All the rotations are out of phase and the average statistical rotation is calculated through the following form:

$$\omega_\alpha = \frac{1}{NM} \sum_i^N \left| \sum_k^M \omega_{i\alpha}^k \right|, \quad (15)$$

where  $M$  is the number of Monte Carlo steps and  $\omega_{i\alpha}^k$  is the rotation along the  $x$ ,  $y$ , or  $z$  axis at site  $i$  for the  $k$  th MC step. It should be noted that the calculated average rotation cannot separate in-phase rotation from out-of-phase rotation. However, it is found that all the rotations are in the out-of-phase mode, which indicates Eq. (15) is enough to describe the

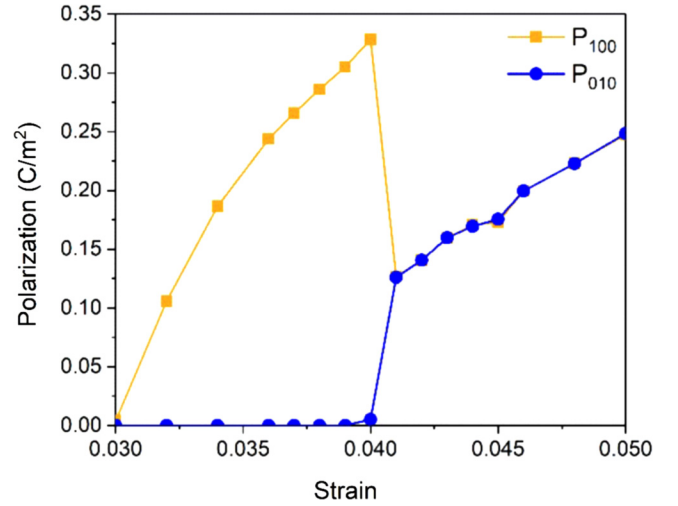


FIG. 5. Polarization changes with in-plane strain under absolute 0 K obtained from the effective Hamiltonian model. The polarization emerges at 3% tensile strain with a [100] direction. When the strain is larger than 4.1%, the value of polarization on [100] direction becomes the same as that on [010] direction, which indicates the polarization points to [110].

oxygen octahedral rotation. The rotation of oxygen octahedra can be described by  $a^0a^0c^-$  (the axis of oxygen octahedral is [001]) according to the Glazer tilt systems [38], when the strain is less than 0.3%. When the tensile strain is larger than 0.3%, the axis of oxygen octahedral rotation changes from [001] to [100]. With the increase of in-plane tensile strain, the rotation changes from [100] to [110]. These phase transitions of oxygen octahedral rotation are similar to that in  $\text{SrTiO}_3$  [39], which also has a path from [001] to [100] and finally achieves [110]. The polarization occurs at 3% tensile strain, and it can reach  $0.350 \text{ C/m}^2$  at 5% tensile strain which is even higher than that of  $\text{BaTiO}_3$ . However, no ferroelectric distortion is found under compressive strain, which is different from that in  $\text{SrTiO}_3$  [15]. This difference mainly arises from the competition between oxygen octahedral rotation and polarization. When the  $\text{BaZrO}_3$  is in-plane compressed, the rotation in the  $z$  direction is enhanced, as is shown in Fig. 4; the average rotation  $\omega_{iz}$  goes up with the strain. And this rotation will suppress the formation of ferroelectricity. Meanwhile, the promotion of ferroelectricity from strain is weak, since it requires as high as  $-2\%$  compressive strain to generate polarization in  $\text{BaZrO}_3$  when rotation is unconsidered [7], while  $\text{SrTiO}_3$  only needs less than  $-1\%$  compressive strain [40]. Furthermore, the  $c/a$  ratios of  $\text{BaZrO}_3$  and  $\text{BaTiO}_3$  with different compressive strains are calculated and compared with the  $c/a$  ratios of  $\text{SrTiO}_3$  from Ref. [41], as shown in Fig. 6. Among these three materials,  $\text{BaTiO}_3$  has polarization under a compressive strain, while  $\text{BaZrO}_3$  has AFD mode and  $\text{SrTiO}_3$  has a phase transition from nonpolar AFD mode to and polar AFD mode. The dash line is the phase boundary of  $\text{SrTiO}_3$ . When the compressive strain is larger than 0.74%, polarization emerges in  $\text{SrTiO}_3$ . Without the participation of polarization, the  $c/a$  ratio grows linear with epitaxial strain. But when the polarization is involved, the growth of the  $c/a$  ratio becomes nonlinear, similar to the behavior of  $\text{BaTiO}_3$  and

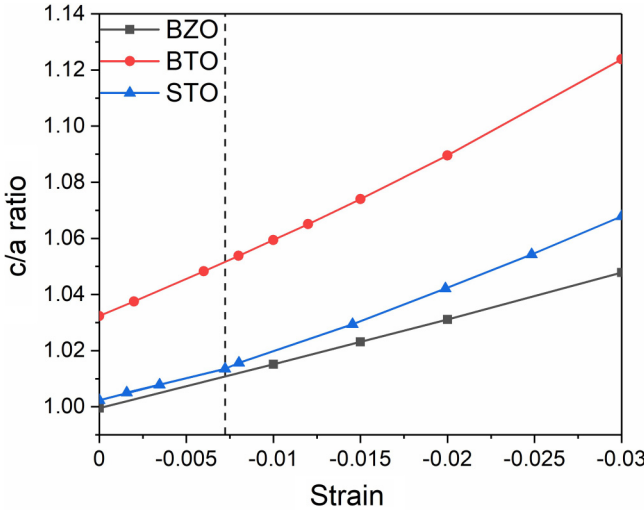


FIG. 6.  $c/a$  ratios of  $\text{BaZrO}_3$ ,  $\text{BaTiO}_3$ , and  $\text{SrTiO}_3$  vary with compressive strain. The  $c/a$  ratios of  $\text{SrTiO}_3$  are taken from Ref. [41]. The dash line is the phase boundary of  $\text{SrTiO}_3$ . When there is only AFD mode,  $c/a$  ratio grows linearly with epitaxial strain, but when the polarization is involved, the growth of  $c/a$  ratio becomes nonlinear.

$\text{SrTiO}_3$  with a larger compressive strain. Thus, the suppression of ferroelectricity is superior to the promotion from strain, and no polarization occurs. When it comes to the tensile strain, as is shown in Fig. 5, it is found from DFT calculations that when the polarization is absent, the rotation in the [100] direction has lower energy than that in the [110] direction, as is shown in Table II. However, after the polarization is considered in the DFT calculations, the polarization and oxygen octahedral rotation favor the [110] direction under a larger tensile strain. These results indicate that there exists a competition between rotation and polarization. When the tensile strain is small, rotation determines the direction of distortion. However, when the strain becomes larger, polarization will replace rotation and dominate the direction of distortion.

### B. Rotation and polarization changes as a function of temperature

Based on the results at absolute zero, how the polarization and oxygen octahedral rotation change with temperature is investigated. Since the melting point of single-crystal  $\text{BaZrO}_3$  can reach as high as 2900 K [40], the model is heated to a relatively higher temperature. During the model heating up to

TABLE II. The energy of different phases from first-principles calculations. 40 atoms (eight unit cells) are used in calculating these modes, and the structure of  $\omega_{100}$  under different strain is regarded as reference state.

Strain	0.02	0.06
$\omega_{100}$	0 eV	0 eV
$\omega_{110}$	$1.28 \times 10^{-03}$ eV	$-1.2 \times 10^{-04}$ eV
$\omega_{100}, P_{010}$		$-5.5932 \times 10^{+01}$ eV
$\omega_{110}, P_{110}$		$-5.6333 \times 10^{+01}$ eV

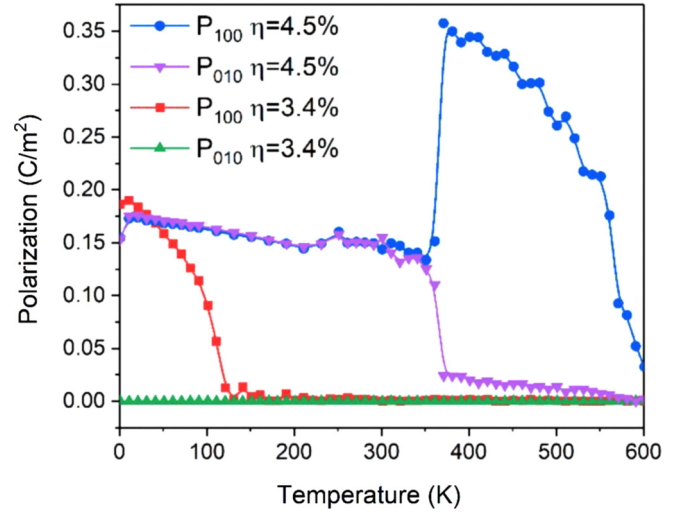


FIG. 7. Polarization changes with temperature under different in-plane strains. When the strain is 3.4%, which is below 4%, the polarization is along [100] direction and vanishes after the model is heated. When the strain is 4.5%, the polarization first points to [110] direction and changes into [100] before it finally disappears.

2000 K from 0 K, both polarization and rotation of oxygen octahedra change with the temperature, which is similar to other materials [42]. Figures 7 and 8 show the temperature dependent polarization and oxygen octahedral rotation under 3.4% and 4.5% tensile strain. When the strain is less than 4.1%, it encounters two phase transitions. The former is due to the vanish of polarization, while the latter is caused by the vanish of oxygen octahedral rotation. The latter phase transition temperature is much larger than the former's, which indicates that the rotation of oxygen octahedra is much more stable than

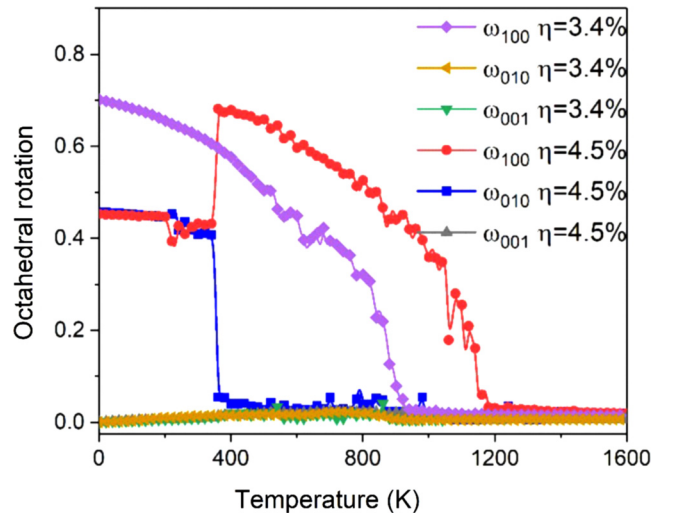


FIG. 8. Rotation of oxygen octahedra changes with temperature. When the strain is 3.4%, which is below 4%, the rotation of oxygen octahedra is in [100] direction and vanishes under a relatively high temperature comparing to the phase transition temperature of polarization. When the strain is 4.5%, the rotation of oxygen octahedra first points to [110] direction and changes into [100] before it finally vanishes.

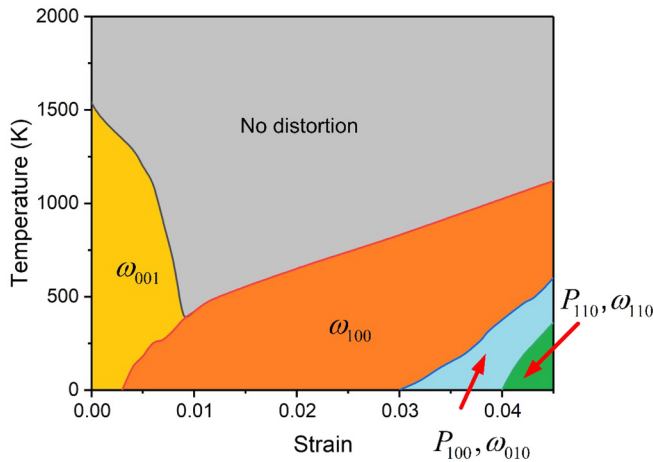


FIG. 9. Strain-temperature phase diagram of BaZrO<sub>3</sub>. The  $P$  and  $\omega$  represent polarization and rotation of oxygen octahedra, while its subscript means the direction.

strain-induced ferroelectricity. When the strain is larger than 4.1%, it goes through three phase transition sequences. First, both polarization and oxygen octahedral rotation changes direction from [110] to [100], then the polarization disappears. And finally, the rotation of oxygen octahedra vanishes. The polarization and rotation of oxygen octahedra change their direction simultaneously, indicating that the direction of polarization is mainly influenced by the coupling between AFD and ferroelectric distortions. Based on these results, the strain versus temperature phase diagram is obtained in Fig. 9. The phase diagram shows that different distortions exhibit in the different strains and temperatures. When the strain is tensile and the temperature is higher than 300 K, there is no distortion, whereas both AFD and ferroelectric distortions are

exhibited at the right-bottom corner of the phase diagram where the temperature is low and the tensile strain is large. It should be noted that the polarization emerges at 3% tensile strain in the present work, which indicates that the ferroelectricity mainly arises from the coupling with strain. Although the LDA functional underestimates lattice parameters and overestimates polarization, its influence on ferroelectricity is very weak compared to the influence of strain.

#### IV. CONCLUSIONS

In summary, the effect of strain and temperature on the AFD and ferroelectric distortions of BaZrO<sub>3</sub> thin films are studied by first-principles calculations and the effective Hamiltonian method. First of all, the unstable phonons of cubic BaZrO<sub>3</sub> are identified, which are employed as the degrees of freedom in the effective Hamiltonian model. Based on the calculated profiles of potential energy, the rotation of oxygen octahedra is responsible for the absence of ferroelectric distortion under compressive strains. Second, the strain dependence of the rotation of oxygen octahedra and polarization is predicted by using an effective Hamiltonian model. It is found that due to the dedicated balance between AFD and ferroelectric distortions, polarization in BaZrO<sub>3</sub> thin films at absolute zero can be activated only under an in-plane tensile strain larger than 3.0%. Finally, the temperature dependence of the rotation of oxygen octahedra and polarization under different strains has been obtained and the strain-temperature phase diagram is constructed to identify the different distortions in BaZrO<sub>3</sub> with different temperatures and strains.

#### ACKNOWLEDGMENTS

This work was financially supported by the National Natural Science Foundation of China (Grant No. 11972320) and Zhejiang Provincial Natural Science Foundation (Grant No. LZ17A020001).

- [1] P. S. Dobal, A. Dixit, R. S. Katiyar, Z. Yu, R. Guo, and A. S. Bhalla, *J. Appl. Phys.* **89**, 8085 (2001).
- [2] D. Pergolesi, E. Fabbri, A. D'Epifanio, E. Di Bartolomeo, A. Tebano, S. Sanna, S. Licoccia, G. Balestrino, and E. Traversa, *Nat. Mater.* **9**, 846 (2010).
- [3] M. Miura, B. Maiorov, T. Kato, T. Shimode, K. Wada, S. Adachi, and K. Tanabe, *Nat. Commun.* **4**, 2499 (2013).
- [4] K. D. Kreuer, *Annu. Rev. Mater. Res.* **33**, 333 (2003).
- [5] A. R. Akbarzadeh, I. Kornev, C. Malibert, L. Bellaiche, and J. M. Kiat, *Phys. Rev. B* **72**, 205104 (2005).
- [6] O. Diéguez, K. M. Rabe, and D. Vanderbilt, *Phys. Rev. B* **72**, 144101 (2005).
- [7] Y. Zhang, M. Liu, J. Wang, T. Shimada, and T. Kitamura, *J. Appl. Phys.* **115**, 224107 (2014).
- [8] D. G. Schlom, L.-Q. Chen, C.-B. Eom, K. M. Rabe, S. K. Streiffer, and J.-M. Triscone, *Annu. Rev. Mater. Res.* **37**, 589 (2007).
- [9] Y. Park, *J. Mater. Sci. Lett.* **17**, 157 (1998).
- [10] D. J. Singh, Q. Xu, and K. P. Ong, *Appl. Phys. Lett.* **104**, 011910 (2014).
- [11] I. A. Kornev, L. Bellaiche, P. Bouvier, P. E. Janolin, B. Dkhil, and J. Kreisel, *Phys. Rev. Lett.* **95**, 196804 (2005).
- [12] R. E. Cohen, *Nature (London)* **358**, 136 (1992).
- [13] K. J. Choi, M. Biegalski, Y. L. Li, A. Sharan, J. Schubert, R. Uecker, P. Reiche, Y. B. Chen, X. Q. Pan, V. Gopalan, L. Q. Chen, D. G. Schlom, and C. B. Eom, *Science* **306**, 1005 (2004).
- [14] C. Ederer and N. A. Spaldin, *Phys. Rev. Lett.* **95**, 257601 (2005).
- [15] J. H. Haeni, P. Irvin, W. Chang, R. Uecker, P. Reiche, Y. L. Li, S. Choudhury, W. Tian, M. E. Hawley, B. Craigo, A. K. Tagantsev, X. Q. Pan, S. K. Streiffer, L. Q. Chen, S. W. Kirchoefer, J. Levy, and D. G. Schlom, *Nature (London)* **430**, 758 (2004).
- [16] Y. L. Li, S. Choudhury, J. H. Haeni, M. D. Biegalski, A. Vasudevarao, A. Sharan, H. Z. Ma, J. Levy, Venkatraman Gopalan, S. Trolier-McKinstry, D. G. Schlom, Q. X. Jia, and L. Q. Chen, *Phys. Rev. B* **73**, 184112 (2006).
- [17] X. Yang, Q. Li, R. Liu, B. Liu, H. Zhang, S. Jiang, J. Liu, B. Zou, T. Cui, and B. Liu, *J. Appl. Phys.* **115**, 124907 (2014).
- [18] M. Guennou, P. Bouvier, J. Kreisel, and D. Machon, *Phys. Rev. B* **81**, 054115 (2010).

- [19] W. Zhong, D. Vanderbilt, and K. M. Rabe, *Phys. Rev. Lett.* **73**, 1861 (1994).
- [20] W. Zhong, D. Vanderbilt, and K. M. Rabe, *Phys. Rev. B* **52**, 6301 (1995).
- [21] S. Bin-Omran, *J. Alloy. Compd.* **674**, 82 (2016).
- [22] J. Iniguez and D. Vanderbilt, *Phys. Rev. Lett.* **89**, 115503 (2002).
- [23] L. Bellaiche, A. García, and D. Vanderbilt, *Phys. Rev. Lett.* **84**, 5427 (2000).
- [24] Igor A. Kornev, L. Bellaiche, P. E. Janolin, B. Dkhil, and E. Suard, *Phys. Rev. Lett.* **97**, 157601 (2006).
- [25] D. Sichuga and L. Bellaiche, *J. Phys.: Condens. Matter* **26**, 025302 (2013).
- [26] Y. Yang, B. Xu, C. Xu, W. Ren, and L. Bellaiche, *Phys. Rev. B* **97**, 174106 (2018).
- [27] B. K. Mani, S. Lisenkov, and I. Ponomareva, *Phys. Rev. B* **91**, 134112 (2015).
- [28] S. Lisenkov, Igor A. Kornev, and L. Bellaiche, *Phys. Rev. B* **79**, 012101 (2009).
- [29] D. Albrecht, S. Lisenkov, Wei Ren, D. Rahmedov, Igor A. Kornev, and L. Bellaiche, *Phys. Rev. B* **81**, 140401(R) (2010).
- [30] G. Song and W. Zhang, *Phys. Rev. B* **94**, 064409 (2016).
- [31] S. Lee, M.-C. Lee, Y. Ishikawa, P. Miao, S. Torii, C. J. Won, K. D. Lee, N. Hur, D.-Y. Cho, and T. Kamiyama, *Phys. Rev. B* **98**, 104409 (2018).
- [32] A. Togo, F. Oba, and I. Tanaka, *Phys. Rev. B* **78**, 134106 (2008).
- [33] S. Baroni, S. de Gironcoli, A. Dal Corso, and P. Giannozzi, *Rev. Mod. Phys.* **73**, 515 (2001).
- [34] X. Gonze and C. Lee, *Phys. Rev. B* **55**, 10355 (1997).
- [35] G. Kresse and J. Furthmüller, *Comput. Mater. Sci.* **6**, 15 (1996).
- [36] W. Zhong and D. Vanderbilt, *Phys. Rev. Lett.* **74**, 2587 (1995).
- [37] A. Bilić and J. D. Gale, *Phys. Rev. B* **79**, 174107 (2009).
- [38] A. M. Glazer, *Acta Crystallogr., Sect. B: Struct. Commun.* **28**, 3384 (1972).
- [39] G. Sheng, Y. L. Li, J. X. Zhang, S. Choudhury, Q. X. Jia, V. Gopalan, D. G. Schlom, Z. K. Liu, and L. Q. Chen, *J. Appl. Phys.* **108**, 084113 (2010).
- [40] C. Xin, P. Veber, M. Guennou, C. Toulouse, N. Valle, M. Ciomaga Hatnean, G. Balakrishnan, R. Haumont, R. Saint Martin, M. Velazquez, A. Maillard, D. Rytz, M. Josse, M. Maglione, and J. Kreisel, *CrystEngComm* **21**, 502 (2019).
- [41] L. Ni, Y. Liu, C. Song, W. Wang, G. Han, and Y. Ge, *Phys. B (Amsterdam, Neth.)* **406**, 4145 (2011).
- [42] W. Zhong and D. Vanderbilt, *Phys. Rev. B* **53**, 5047 (1996).